



# Synthesis, crystal structure, spectroscopic properties, antibacterial activity and theoretical studies of a novel difunctional acylhydrazone

Yan-Xian Jin <sup>a,\*</sup>, Ai-Guo Zhong <sup>a</sup>, Yu-jian Zhang <sup>b</sup>, Fu-You Pan <sup>a</sup>

<sup>a</sup> School of Pharmaceutical and Chemical Engineering, Taizhou University, Linhai 317000, PR China

<sup>b</sup> State Key Laboratory Breeding Base of Green Chemistry-Synthesis Technology, College of Chemical Engineering and Materials Science, Zhejiang University of Technology, Chaowang Road 18#, Hangzhou 311000, PR China

## ARTICLE INFO

### Article history:

Received 9 May 2011

Received in revised form 15 June 2011

Accepted 27 June 2011

Available online 3 July 2011

### Keywords:

ILCT

Fluorescence property

Antibacterial activity

Quantum calculation

## ABSTRACT

A novel difunctional acylhydrazone has been synthesized by the reaction of 5-methylisoxazole-4-carboxyl hydrazine with benzaldehyde and characterized by X-ray crystallography and spectroscopy. The obtained results demonstrate the crystal belongs to triclinic, space group  $P\bar{1}$ . Moreover, the spectroscopic properties were evaluated through density functional theory (DFT) and time-dependent density functional theory (TD DFT) calculations. The results reveal that UV-Vis absorption peaks at 194, 217.5 and 290.5 nm are mainly attributed to  $(p, \pi) \rightarrow \pi^*$ , partly  $(p, \pi) \rightarrow \pi^*$  and partly  $\pi \rightarrow \pi^*$ , and predominantly  $\pi \rightarrow \pi^*$ , respectively, with intraligand charge-transfer transition (ILCT) character. The fluorescence emission peak at 485.96 nm should be assigned to ILCT. In addition, the results of antibacterial activities indicate the title compound has certain modest antibacterial activity as well as the broad-spectrum bacteriostasis, which can be supported by the molecular electrostatic potential (MEP). Therefore, the title compound exhibits both antibacterial activity and photoluminescent property, which has potential applications in many fields such as material science and photodynamic therapy.

© 2011 Elsevier B.V. All rights reserved.

## 1. Introduction

Hydrazones, which are usually prepared via the condensation of aldehydes or ketones with hydrazines, are well known to be biologically important and interest in studying this class of compound lies in its antibacterial, antitumour and antitubercular activities [1]. In addition, it has been used as an analytical reagent [2] and as polymer-coating, ink, pigment [3] and fluorescent materials [4]. Previous studies have focused on their extraordinary ability to form complexes with metal ions and multiform in the complexes, as well as exploring to develop new drugs based on their biological properties [5]. For instance, Ainscough et al. [5] had extensively studied the coordination chemistry of acylhydrazones as well as the molecule of a number of copper(II) complexes. Similarly, Singh et al. [5] synthesized the cobalt(II) complexes with some acylhydrazones, which showed a fair antifungal and antibacterial activity against a number of fungi and bacteria. Otherwise, photoluminescence, photoabsorption and photoemission studies of hydrazone thin film used as hole transporting material in organic light emitting diodes (OLEDs) was reported [6].

On the other hand, isoxazole compounds have a rich history with both pharmaceutical and agricultural applications due to their apoptotic activity [7], plant-growth regulating activity [8]

and antibacterial activity [9]. To the best of our knowledge, however, compounds containing both the acylhydrazone and isoxazole functional groups have been an underdeveloped area. Furthermore, we could not find any related studies about acylhydrazones that analyze the relation between the structure and photic properties or antibacterial activity by the means of quantum calculation.

In order to broaden the application of hydrazones and explore new functional materials, the novel compound containing both the acylhydrazone and isoxazole groups, (*E*)-*N'*-benzylidene-5-methylisoxazole-4-carbohydrazide, was designed and prepared. The scheme of the molecule is as followed (see Scheme 1):

We have now taken on general investigation of the synthesis, crystal structure, absorption, luminescent and antibacterial properties of the title compound. Besides, the electronic structure, absorption spectroscopic nature and photoluminescent mechanism with molecular orbital calculations have been explored by using quantum mechanical computational tools from density functional theory (DFT), and time-dependent density functional theory (TD DFT). The results are reported in the paper.

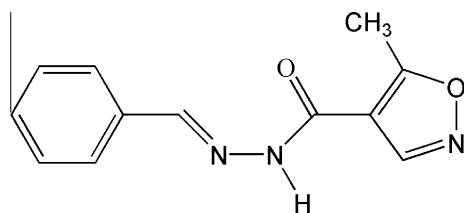
## 2. Experimental

### 2.1. Materials and methods

All solvents and chemicals were commercial reagents and used without further purification. IR spectra were recorded on a Nicolet

\* Corresponding author. Tel.: +86 576 85137265.

E-mail address: [snowflakej@gmail.com](mailto:snowflakej@gmail.com) (Y.-X. Jin).



**Scheme 1.** The scheme of the molecule of the title compound.

FT-IR 170X spectrophotometer with KBr pellets in the range of 4000–400  $\text{cm}^{-1}$ .  $^1\text{H}$  NMR spectra were measured with a Varian XL200 nuclear magnetic resonance spectrometer using acetone- $\text{d}_6$  as solvent and tetramethylsilane as an internal standard. UV–Vis spectra were recorded on a Shimadzu UV-2401PC spectrometer. Fluorescence spectra were measured on a F-4500 fluorescence spectrometer.

## 2.2. Synthesis of the title compound

Benzaldehyde (4.6 g, 0.02 mol) and 5-methylisoxazole-4-carbonyl hydrazine (2.8 g, 0.02 mol) was mixed with glacial acetic acid (50 mL). The mixture was heated at 65 °C for 3 h, the precipitate collected by filtration and washed with water, chloroform and ethanol. The product was recrystallized from ethanol, and then dried under reduced pressure to give the desired compound in 85% yield. Colorless, block-shaped crystals were obtained by slow evaporation of a dimethylformamide solution.  $^1\text{H}$  NMR ( $\text{CD}_3\text{COCD}_3$ , 200 MHz),  $\delta$  2.68 (s, 3H,  $-\text{CH}_3$ ), 7.2–7.8 (m, 5H, Ar–H), 8.2 (s, 1H,  $-\text{N}=\text{CH}-$ ), 8.8 (s, 1H, 3-isoxazole-H), 10.6 (s, 1H,  $-\text{CO}-\text{NH}-$ ). IR (KBr)  $\nu$ : 3175.6 (N–H), 1651.0 (C=O), 1593.1 (C=N). MS(ESI):  $m/z$  229.3.

## 2.3. X-ray structure determination

A single colorless crystal of the title compound having approximate dimensions of 0.22 mm  $\times$  0.19 mm  $\times$  0.08 mm was mounted on the top of a glass fiber in a random orientation. All X-ray crystallographic data were collected on a Bruker SMART APEX II CCD diffractometer equipped with a graphite-monochromatized Mo  $K\alpha$  radiation ( $\lambda = 0.71073 \text{ \AA}$ ) radiation using the  $\phi/\omega$  scan technique at 293 K. The structures were solved by a direct method and refined by a full-matrix least-squares procedure based on  $F^2$  using the SHELXTL program package [10]. An empirical absorption correction was applied with the program SADABS [10]. The H atom bound to N2 was located in a different Fourier map and refined freely with the N–H distance restrained to 0.90  $\text{\AA}$ . All other H atoms were positioned geometrically and allowed to ride on their parent atoms. The weighted  $R$ -factor  $wR$  and goodness of fit  $S$  are based on  $F^2$ , conventional  $R$ -factors  $R$  are based on  $F$ , with  $F$  set to zero for negative  $F^2$ . The threshold expression of  $F^2 > \sigma(F^2)$  is used only for calculating  $R$ -factors ( $gt$ ), etc. and is not relevant to the choice of reflections for refinement.  $R$ -factors based on  $F^2$  are statistically about twice as large as those based on  $F$ , and  $R$ -factors based on all data will be even larger. Crystallographic data and experimental details of the structure determinations are listed in Table 1. CCDC Deposition No: CCDC 755458.

## 2.4. Computational method

Optimized calculations of the title compound in the ground state ( $S_0$ ) were done at the DFT B3LYP/6-31G(d) level [11] within the Gaussian 03W software package [12]. Absorption spectra (UV–Vis) based on the above DFT-optimized structures were obtained by the time-dependent density functional theory (TD

**Table 1**  
Crystallographic and data collection parameters for the title compound.

Empirical formula	$\text{C}_{12}\text{H}_{11}\text{N}_3\text{O}_2$
Formula weight	229.24
Crystal system	triclinic
Space group	$P\bar{1}$
$a, b, c$ ( $\text{\AA}$ )	6.6562(6), 7.4874(9), 11.3051(11)
$\alpha, \beta, \gamma$ ( $^\circ$ )	87.319 (8), 84.640 (7), 87.878 (8)
$V$ ( $\text{\AA}^3$ )	560.04(10)
$Z$	2
$\rho_{\text{calc.}}$ ( $\text{g cm}^{-3}$ )	1.359
$R[F^2 > 2\sigma(F^2)]$	0.095
$wR(F^2)$ [all data]	0.302
Min., max. $\Delta\rho$ ( $\text{e \AA}^{-3}$ )	–0.34, +0.53

DFT B3LYP) level [13] with the 6-311+G(d) basis set. Meanwhile, the fluorescence spectrum of the obtained compound has been calculated by TD DFT/6-311+G(d) [14], based on the optimized structure of excited-state ( $S_1$ ) by HF CIS/6-31+G(d) [15].

## 2.5. Antibacterial activities

Using suitable stains of *Bacillus subtilis*, *Pseudomonas aeruginosa*, *Escherichia coli* and *Staphylococcus aureus* (obtained from Taizhou hospital, Zhejiang Province), the sensitivity of microorganisms in the title compound was detected by means of Kirby–Bauer disc agar diffusion test. The culture medium was beef extract peptone medium. Bacteria are active in slant medium, cultured in liquid medium for 16 h at 37 °C and diluted with liquid medium before use by a ratio of 1000. The compound was made up to the desired concentration with DMF and a 6 mm diameter disc of filter paper was immersed into this solution. The disc was put on the agar culture dish, which was then spread with the appropriate microorganism. The dish was cultured for 24–28 h at 37 °C and the diameter of halo around the disc was measured. In parallel, tests with DMF blank and streptomycin sulfate positive control were completed.

## 3. Results and discussion

### 3.1. Molecular and crystal structure of the title compound

The molecule of the obtained compound,  $\text{C}_{12}\text{H}_{11}\text{N}_3\text{O}_2$ , is approximately planar with an r.m.s. deviation of 0.0814  $\text{\AA}$  from the plane through all the non-H atoms. The dihedral angle formed by the benzene (C7–C12) and isoxazole rings (C2–C4, N1, O1) is 6.88 ( $16^\circ$ ) (Fig. 1). The molecule displays an  $E$  conformation with respect to the C6=N3 double bond, with a C7–C6–N3–N2 torsion angle of  $-179.3(3)^\circ$ . The intramolecular C3–H3 $\cdots$ N3 and C8–H8 $\cdots$ N3 hydrogen bonds generate S6 and S5 ring motifs, respectively, which lock the molecule into planar conformation (Fig. 2). Bond lengths and angles are unexceptional and similar to those found in related structures [16].

In the crystal structure (Fig. 2), intermolecular N2–H2 $\cdots$ O2 hydrogen bonds form centrosymmetric dimers. These are further linked by weak C1–H1B $\cdots$ N1 interactions augmented by very weak, inversion related C1–H1A $\cdots$ Cg1 contacts to form layers parallel to (120) (Cg1 is the centroid of the C7 $\cdots$ C12 phenyl ring). The geometry of the fragment D–H $\cdots$ A for the title compound is shown in Table 2.

The Gaussian 03W suite of programs is employed to optimize the geometries of the title compound [12]. Geometric configuration in ground state ( $S_0$ ) are optimized by B3LYP method at the level of 6-31G(d). As shown in Table 3, the calculated values of bond length and bond angle of the title compound are in good agreement with the experimental data.

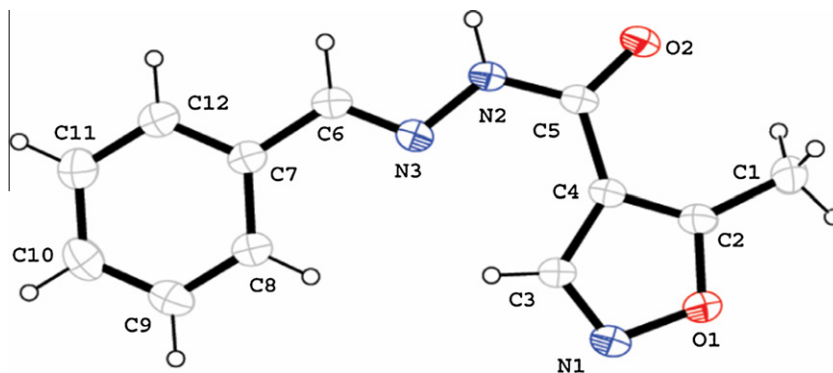


Fig. 1. Molecular structure of the title compound. Displacement ellipsoids are drawn at the 30% probability level. H-atoms are depicted as spheres of arbitrary radii.

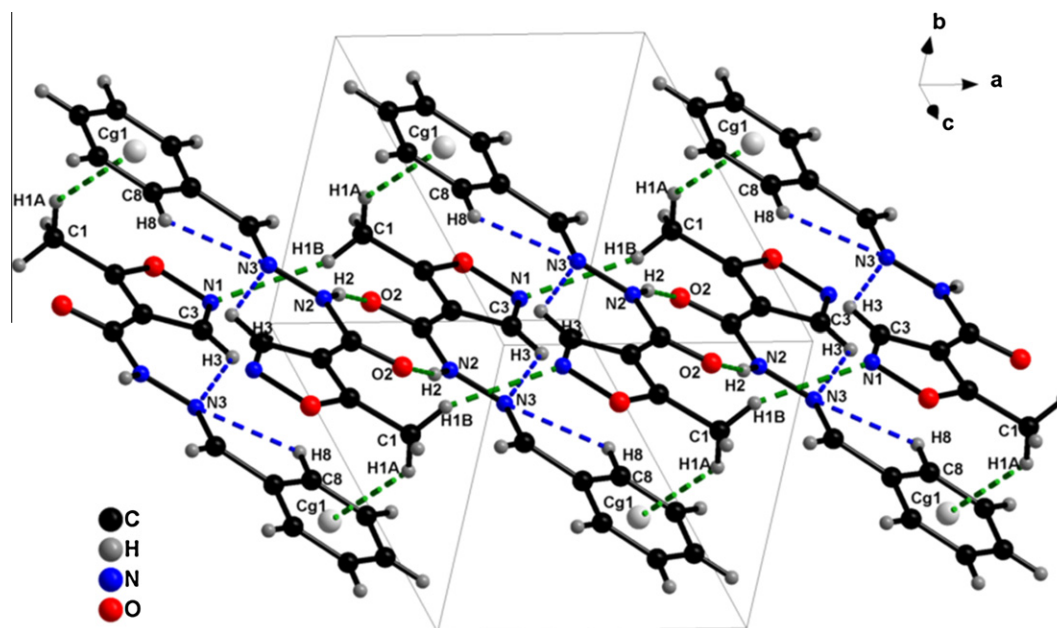


Fig. 2. Packing diagram of the title compound. Intermolecular and intramolecular hydrogen bonds are shown as dashed lines.

Table 2

The geometry of the fragment  $D-H\cdots A$  for the title compound [bond length ( $d$ ) in Å, bond angle ( $\angle DHA$ ) in  $^\circ$ ].

$D-H\cdots A$	$d(D-H)$	$d(H\cdots A)$	$d(D\cdots A)$	$\angle DHA$
C(3)—H(3A) $\cdots$ N(3)	0.93	2.39	2.893(5)	114
C(8)—H(8) $\cdots$ N(3)	0.93	2.61	2.877	97.4
N(2)—H(2) $\cdots$ O(2) <sup>i</sup>	0.90(1)	1.98(1)	2.867(4)	170(4)
C(1)—H(1B) $\cdots$ N(1) <sup>ii</sup>	0.96	2.67	3.598(6)	162
C(1)—H(1B) $\cdots$ C(g1) <sup>iii</sup>	0.96	3.35	4.136(7)	140

Symmetry codes: (i)  $-x, -y + 1, -z + 1$ ; (ii)  $x - 1, y, z$ ; (iii)  $-x + 1, -y + 1, -z + 1$ . Cg1 is the centroid of the C7—C12 ring.

### 3.2. Frontier molecular orbitals and electronic spectrum

To investigate the electronic and luminescent properties of the title compound, we carried out molecular orbital calculations based on the optimized ground state geometries. Frontier orbitals play an important role because they rule the electronic excitation and transition character [17]. Thus, the most important ground state frontier molecular orbitals of the title compound are listed in Table 4. Furthermore, to further find out the properties of absorption spectra, the UV–Vis absorption spectrum was

Table 3

The optimized bond length (Å) and bond angle ( $^\circ$ ) of the title compound compared with the experimental data.

Parameters	Exp.	Cal.	Parameters	Exp.	Cal.
C(2)—O(1)	1.337(4)	1.329	C(6)—N(3)	1.269(5)	1.282
C(2)—C(4)	1.352(5)	1.375	C(6)—C(7)	1.464(5)	1.450
C(3)—N(1)	1.288(5)	1.302	C(9)—C(10)	1.374(6)	1.386
C(3)—C(4)	1.417(5)	1.416	C(10)—C(11)	1.373(6)	1.391
C(4)—C(5)	1.473(5)	1.450	C(11)—C(12)	1.373(6)	1.384
C(5)—O(2)	1.239(4)	1.226	N(1)—O(1)	1.412(4)	1.387
C(5)—N(2)	1.336(5)	1.374	N(2)—N(3)	1.373(4)	1.328
O(1)—C(2)—C(4)	109.7(3)	109.06	N(2)—C(5)—C(4)	121.4(3)	122.6
O(1)—C(2)—C(1)	115.1(3)	117.84	N(3)—C(6)—C(7)	121.8(3)	122.19
C(4)—C(2)—C(1)	135.3(4)	133.10	C(12)—C(7)—C(8)	117.9(4)	119.17
N1—C(3)—C(4)	113.2(3)	112.11	C(12)—C(7)—C(6)	119.8(4)	119.17
C(2)—C(4)—C(3)	103.5(3)	103.24	C(8)—C(7)—C(6)	122.2(3)	121.87
C(2)—C(4)—C(5)	123.5(3)	122.11	C(3)—N(1)—O(1)	104.4(3)	105.35
C(3)—C(4)—C(5)	133.0(3)	134.65	C(5)—N(2)—N3	123.3(3)	125.12
O(2)—C(5)—N(2)	118.7(3)	118.33	C(6)—N(3)—N(2)	115.5(3)	117.83
O(2)—C(5)—C(4)	119.9(3)	122.60	C(2)—O(1)—N(1)	109.3(3)	110.14

simulated. As shown in Fig. 3, the first absorption peak located at 198 nm (calculated) is correlated with the 194 nm peak in the experimental UV–Vis spectrum. In terms of the molecular orbital

**Table 4**  
Electronic absorption data and frontier molecular orbitals obtained by TD-DFT/6-311+G(d)//DFT B3LYP 6-31G(d) method in water.

States	$\Delta E$ (eV)	$\lambda$ (nm)	$f$ (a.u.)	Assignment	Molecular orbitals
$S_1$	4.13	299.6	0.865	HOMO $\rightarrow$ LUMO (91%) ( $\pi \rightarrow \pi^*$ )	
$S_2$	5.65	221.2	0.476	HOMO $\rightarrow$ LUMO + 2 (36%) ( $\pi \rightarrow \pi^*$ )	
				HOMO-2 $\rightarrow$ LUMO (32%) (p, $\pi \rightarrow \pi^*$ )	
$S_3$	6.32	198.0	0.419	HOMO-2 $\rightarrow$ LUMO + 1 (54%) (p, $\pi \rightarrow \pi^*$ )	

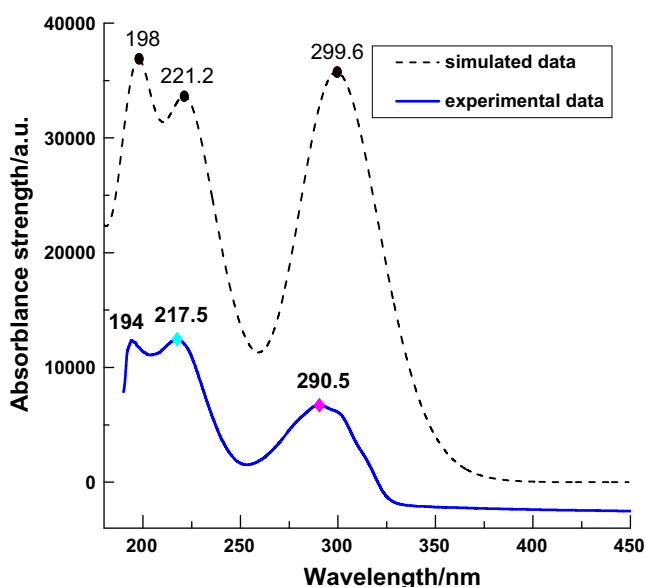


**Fig. 3.** The simulated and experimental UV-Vis absorption spectra of the title compound by TD DFT/6-311+G(d)//DFT B3LYP 6-31G(d) method in water.

analysis, it is primarily associated with the transition from Highest Occupied Molecular Orbital for HOMO-2 to Lower Unoccupied Molecular Orbital for LUMO + 1 with configuration interaction coefficient up to 0.54. Because of the  $\pi$  orbital character of the isoxazole ring and p orbitals of O and N atoms for HOMO-2, and the  $\pi^*$  antibonding orbitals character of isoxazole ring for LUMO + 1, the transition can be ascribed to (p,  $\pi$ )  $\rightarrow$   $\pi^*$ , intraligand charge-transfer transition (ILCT). The second calculated absorption at 221.2 nm can be correlated to the 217.5 nm band in the experimental UV-Vis spectrum. It mainly arises from HOMO to LUMO + 2 with configuration interaction coefficient up to 0.36 and from HOMO-2 to LUMO with configuration interaction coefficient up to 0.32. HOMO is predominantly the  $\pi$  orbital character of isoxazole and benzene ring, LUMO + 2 is completely the  $\pi^*$  antibonding orbital character of benzene ring, while HOMO-2 shows the  $\pi$  orbital character (mentioned above) and LUMO is primarily the  $\pi^*$  antibonding orbital character of benzene ring, therefore, the transition can be reasonably attributed to  $\pi \rightarrow \pi^*$  and (p,  $\pi$ )  $\rightarrow$   $\pi^*$  with character ILCT. The simulated third absorption maximum at 299.6 nm can be readily correlated with 290.5 nm peak in the experimental spectrum. The transition mostly originates from HOMO to LUMO with a maximum configuration interaction coefficient of 0.91 and this

transition is reasonably  $\pi \rightarrow \pi^*$ , ILCT. Fortunately, a comparison by TD DFT calculated and experimental absorption spectrum shows the calculated results are in fairly good agreement with the experimental ones.

### 3.3. Luminescence property and emission spectra

The luminescent property in water with the concentration of  $1 \times 10^{-4}$  mol/L was measured at room temperature. As shown in Fig. 4, the obtained compound exhibits strong green emission with a peak at 485.96 nm, which is excited at 210.0 nm.

Meanwhile, the fluorescence spectrum was also calculated by TD-pbepbe/6-311+G(d) in water, based on the optimized structure of excited-state ( $S_1$ ) by HF CIS/6-31+G(d), the results indicate that the theoretical emission peak located at 486.7 nm is fully consistent with the experimental values.

According to the TD DFT energy level and molecular orbital analysis,  $S_1 \rightarrow S_0$  transitions was mainly associated with the transitions from the corresponding LUMO  $\rightarrow$  HOMO, owing to their largest configuration coefficients up to 0.99. Because the LUMO is predominated  $\pi$  bonding orbital of isoxazole ring, while HOMO is  $\pi^*$  antibonding orbitals of benzene ring, the emission peaks located at 485.96 nm should be assigned to ILCT.

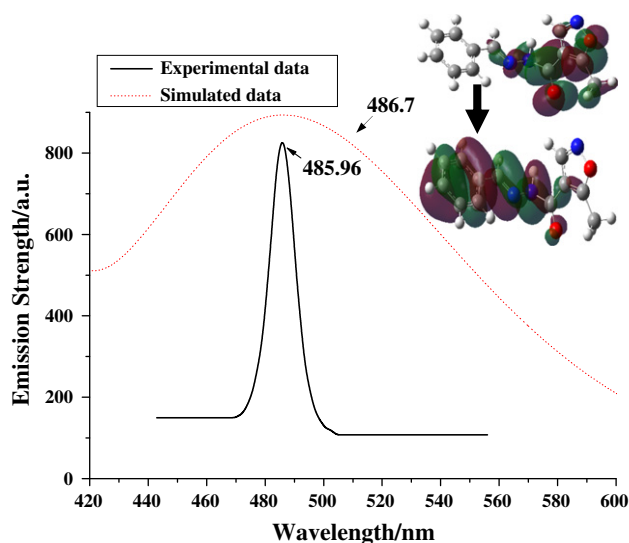


**Fig. 4.** The simulated and experimental emission spectra of the title compound at TD DFT/pbepbe/6-311+G(d)//HF CIS/6-31+G(d) in water.

**Table 5**

Antibacterial activity of the title compound and the similar compound (diameter of antibacterial halo in mm).

Compounds	<i>B. subtilis</i>	<i>P. aeruginosa</i>	<i>E. coli</i>	<i>S. aureus</i>
The title compound <sup>a</sup>	8.12	10.67	6.97	8.22
DMF	5.94	5.94	5.94	5.94
Streptomycin sulfate	28.00	20.70	22.00	23.50
Similar compound from the reference <sup>b</sup> [18]	6.00	6.00	9.50	8.50
Streptomycin sulfate [18]	27	26	27	30

Note: 6–8, 8–12, 12–16 and 16–20 mean the faint antibacterial activity, weak antibacterial activity, moderate antibacterial activity, strong antibacterial activity, respectively. Diameter of antibacterial halo in mm.

<sup>a</sup> The concentration of the compound used in the sensitive test was 7 mg mL<sup>-1</sup>. Strains of streptomycin sulfate concentration was 100 units/mL.

<sup>b</sup> The concentration of the compound used to *B. subtilis* and *S. Aureus* was 1 mg mL<sup>-1</sup>, to other two bacteria was 10 mg mL<sup>-1</sup>.

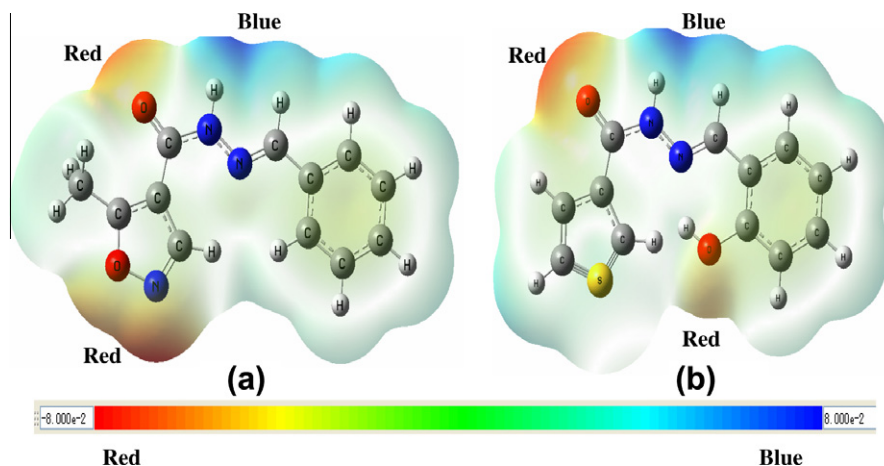


Fig. 5. Electrostatic potential maps of: (a) the title molecule and (b) the similar compound in Ref. [18] (red color for the negative and blue color for positive charge).

### 3.4. The activity data of antibacterial and molecular electrostatic potential

Different conformations of hydrazones may show different biological activities. The antibacterial activities of the compound and the similar compound are listed in Table 5, as estimated by the diameter of antibacterial halo. The title compound shows weak activity towards *B. subtilis*, *P. aeruginosa*, and *S. aureus* and faint antibacterial activity for *E. coli*, indicating that this type of compound has certain modest antibacterial activity. It is worthy noting that the obtained compound has broad spectrum activity against Gram-positive and Gram-negative bacteria compared to the similar compound [18].

An advantage to use of the molecular electrostatic potential (MEP) as a representation of the electrostatic potential is that it provides a direct visual comparison of results. The MEP plots could show regions ranging from negative (red color)<sup>1</sup> to positive (blue color) electrostatic potentials as an indicator of the charge distribution in a molecule, where the regions with higher negative (positive) values of  $V(r)$  are richer (more lacking) in electron density. As a result, MEP was frequently used to point to atoms suitable for electrophilic or nucleophilic attack [19].

The MEP maps of the title molecule and a similar compound in reference [18] are shown in Fig. 5, and the values of the electrostatic potentials (in atomic units) are indicated in the scale (shown in the bottom of Fig. 5). The most striking difference between the two molecular surfaces is the potential distribution on the active sites. The negative electrostatic potential points (red color) for nucleophilic attack (electron donor sites) focus on the surface of

atoms O(2), N(1) and O(1) in the title compound (Fig. 5a), whereas the negative electrostatic potential points concentrate on the two O atoms in the similar compound (Fig. 5b). It is evident that the former has more negative electrostatic potential points than the latter. On the other hand, the positive (blue) electrostatic potential sites for electrophilic attack (electron acceptor sites) on the surface of H atoms bound to N(2) and N(3) in the desired molecule (Fig. 5a) are found no significant difference in comparison with the corresponding part in the similar compound (Fig. 5b). Consequently, the more aggression sites of the nucleophile or nucleophilic attack in the title compound, used to rationalize the interaction between a biological active compound and its biomacro-molecular target [19], maybe have some connection with the broad spectrum activity against Gram-positive and Gram-negative bacteria compared to the similar compound.

## 4. Conclusions

A novel difunctional isoxazole-acylhydrazone has been synthesized and its geometric structure, electronic structure and spectroscopic properties were thoroughly investigated by X-ray crystallography, spectroscopic investigation, DFT and TD DFT theoretical approaches. In accordance with our experiments, the TD DFT calculations show that absorption peaks at 194, 217.5 and 290.5 nm are mainly attributed to  $(p, \pi) \rightarrow \pi^*$ , partly  $(p, \pi) \rightarrow \pi^*$  and partly  $\pi \rightarrow \pi^*$ , and predominantly  $\pi \rightarrow \pi^*$ , respectively, all of which are with ILCT character. The title compound gives rise to strong green fluorescence with a peak at 485.9 nm, which should be assigned to ILCT. What's more, the results of antibacterial activities demonstrate the title compound has certain modest antibacterial activity as well as the broad spectrum bacteriostasis. Meanwhile, the molecular electrostatic potential (MEP) has been calculated to

<sup>1</sup> For interpretation of color in Fig. 5, the reader is referred to the web version of this article.

support its broad-spectrum antibacterial activity. Therefore, the title compound has both the antibacterial activity and photoluminescent property, namely difunctionality, suggesting that it has potential applications in many fields such as material science and photodynamic therapy.

## Acknowledgements

We thank the Center-Laboratory for Computational Chemistry of Taizhou College, for allowing us to access its computing facilities for the present study. The project was supported by the Natural Science Foundation of Zhejiang Province, China (Y 4110348).

## References

- [1] (a) S.G. Küçükgül, E.E. Oruç, S. Rollas, F. Sahin, A. Özbek, *Eur. J. Med. Chem.* 37 (2002) 197;  
(b) A.S. El-Tabl, F.A. El-Saied, A.N. Al-Hakimi, *J. Coord. Chem.* 61 (2008) 2380;  
(c) C. Alvarez, R. Alvarez, P. Corchete, J.L. Lopez, C. Perez-Melero, R. Pelaez, M. Medarde, *Bioorg. Med. Chem.* 16 (2008) 5952;  
(d) C. Ventura, F. Martins, *J. Med. Chem.* 51 (2008) 612.
- [2] R.M. El-Bahnasawy, A.S. El-Tabl, E. El-Shereafy, T.I. Kashar, Y.M. Issa, *Pol. J. Chem.* 73 (1999) 1952.
- [3] D.F. Martin, G.A. Jamusonis, B.B. Martin, *J. Am. Chem. Soc.* 83 (1961) 73.
- [4] (a) F.-F. Tian, F.-L. Jiang, X.-L. Han, C. Xiang, Y.-S. Ge, J.-H. Li, Y. Zhang, R. Li, X.-L. Ding, Y. Liu, *J. Phys. Chem. B* 114 (2010) 14842;  
(b) S.K. Agrawal, R. Chandra, *Proc. Natl. Acad. Sci.* 55 (A) (1985) 11;  
(c) S. Hapuarachchige, G. Montaña, C. Ramesh, D. Rodriguez, L. Hen, C.C. Williams, S. Kadavakkollu, D.L. Johnson, C.B. Shuster, J.B. Arterburn, *J. Am. Chem. Soc.* 133 (2011) 6780.
- [5] (a) E.W. Ainscough, A.M. Brodie, J.D. Ranford, J.M. Waters, *Inorg. Chim. Acta* 236 (1995) 83;  
(b) E.W. Ainscough, A.M. Brodie, A.J. Dobbs, J.D. Ranford, J.M. Waters, *Inorg. Chim. Acta* 267 (1998) 27;  
(c) S.C. Chan, L.L. Koh, P.H. Leung, J.D. Ranford, K.Y. Sim, *Inorg. Chim. Acta* 236 (1995) 101;  
(d) C. Manzur, L. Millán, W. Figueroa, D. Boys, J.R. Hamon, D. Carrillo, *Organometallics* 22 (2003) 153;  
(e) V.P. Singh, A. Singh, *Russ. J. Coord. Chem.* 34 (2008) 374.
- [6] W.G. Quirino, C. Legnani, M. Cremona, R. Reyes, G.V. Mota, D.E. Weibel, M.L.M. Rocco, *J. Braz. Chem. Soc.* 19 (2008) 872.
- [7] D. Simoni, M. Roberti, F.P. Invidiata, R. Rondanin, R. Baruchello, C. Malagutti, A. Mazzali, M. Rossi, S. Grimaudo, F. Capone, L. Dusonchet, M. Meli, M.V. Raimondi, M. Landino, N. D'Alessandro, M. Tolomeo, D. Arindam, S.N. Lu, D.M. Benbrook, *J. Med. Chem.* 44 (2001) 2308.
- [8] J.B. Carr, H.G. Durham, D.K. Hass, *J. Med. Chem.* 20 (1977) 934.
- [9] F.E. Dayan, S.O. Duke, K.N. Reddy, B.C. Hamper, K.L. Leschinsky, *J. Agric. Food Chem.* 45 (1997) 967.
- [10] (a) G.M. Sheldrick, *SHELXTL Software Reference Manual*, Version 5.1, Bruker AXS Inc., Madison, Wisconsin, USA, 1997.;  
(b) Siemens, *SAINTE*, Area Detector Control and Integration Software, Siemens Analytical X-ray Instruments Inc., Madison, Wisconsin, USA, 2002.;  
(c) G.M. Sheldrick, *SADABS*, Program for Empirical Absorption Correction of Area Detector Data, University of Göttingen, Germany, 2002.
- [11] (a) A. Klanicová, Z. Trávníček, I. Popa, M. Čajan, K. Doležal, *Polyhedron* 25 (2006) 1421;  
(b) F.A. Momany, J.L. Willett, *J. Comput. Chem.* 21 (2000) 1204.
- [12] M.J. Frisch, G.W. Trucks, H.B. Schlegel, et al., *GAUSSIAN 03*, Revision B.01[CP], Gaussian, Inc., Pittsburgh, PA, 2003.
- [13] (a) E. Runge, E.K.U. Gross, *Phys. Rev. Lett.* 52 (1984) 997;  
(b) M.E. Casida, C. Jamorski, K.C. Casida, D.R. Salahub, *J. Chem. Phys.* 108 (1998) 4439;  
(c) M.E. Casida, in: D.P. Chong (Ed.), *Recent Advances in Density Functional Methods*, vol. 1, World Scientific, Singapore, 1995, p. 155;  
(d) C. Adamo, G.E. Scuseria, V. Barone, *J. Chem. Phys.* 111 (1999) 2889;  
(e) S. Hirata, M. Head-Gordon, R.J. Bartlett, *J. Chem. Phys.* 111 (1999) 10774.
- [14] H. Wang, X. Wang, X. Li, C. Zhang, *J. Mol. Struct.: THEOCHEM* 770 (2006) 107.
- [15] H. Wang, X. Wang, C. Zhang, *J. Mol. Struct.: THEOCHEM* 819 (2007) 60.
- [16] F.H. Allen, O. Kennard, D.G. Watson, L. Brammer, A.G. Orpen, R. Taylor, *J. Chem. Soc.* (1987) 1.
- [17] X.-N. Li, J.-K. Feng, A.-M. Ren, L.-J. Li, *Synth. Met.* 157 (2007) 1046.
- [18] J.-G. Yang, F.-Y. Pan, J.-M. Li, *Chin. J. Inorg. Chem.* 21 (2005) 1593.
- [19] (a) G.M. Gehad, M.S. Carmen, *Spectrochim. Acta Part A: Mol. Biomol. Spectrosc.* 66 (2007) 949;  
(b) F. Tielens, *J. Mol. Struct.: THEOCHEM* 903 (2009) 23;  
(c) P. Brown, D.J. Best, N.J.P. Broom, R. Cassels, P.J. O'Hanlon, T.J. Mitchell, N.F. Osborne, J.M. Wilson, *J. Med. Chem.* 40 (1997) 2563–2570.